The Astro-E/XRS Calibration Program and Results

Keith C. Gendreau[a,b], M. Damian Audley[c], Keith A. Arnaud[a,b],
Kevin R. Boyce[b], Ryuichi Fujimoto[c], Yoshitaka Ishisaki[d],
Richard L. Kelley[b], Tatehiro Mihara[e], Kazuhisa Mitsuda[c],
F. Scott Porter[b], Caroline K. Stahle[b], and Andrew E. Szymkowiak[b]

[a]Univerisity of Maryland, College Park MD, USA
[b]Goddard Space Flight Center, Greenbelt MD, USA
[c]Institute of Space and Astronautical Sciences, Sagamihara, Japan
[d]Tokyo Metropolitan University, Japan
[e]The Institute of Physical and Chemical Research (RIKEN), Japan

ABSTRACT

XRS is the microcalorimeter X-ray detector aboard the US-Japanese ASTRO-E observatory, which is scheduled to be launched in early 2000. XRS is a high resolution spectrometer- with less than 9 eV resolution at 3 keV and better than 14 eV resolution over its bandpass ranging from about 0.3 keV to 15 keV. Here we present the results of our first calibration of the XRS instrument. We describe the methods used to extract detailed information about the detection efficiency and spectral redistribution of the instrument. We also present comparisons of simulations and real data to test our detector models.

Keywords: X-ray, Calibration, Calorimeter, Spectrometer

1. INTRODUCTION

The XRS (X-ray Spectrometer) instrument is the prime focal plane instrument of the Japan/US X-ray astronomy mission Astro-E. Astro-E will be Japan's 5th satellite devoted to X-ray astrophysics. For more details on Astro-E, see Ogawara, 1998 [1]. The XRS instrument is an X-ray microcalorimeter which will produce high quality spectra in the 0.4 to 15 keV bandpass out of photons collected by an X-ray telescope dedicated to XRS. The heart of XRS consists of 32 extremely sensitive thermometers. Attached to these thermometers are small ($8 \times 1236 \times 314$ microns) HgTe wafers that serve as X-ray absorbers. This focal plane is kept at 60 mK (with a stability of about 10 microkelvin) using a complex refrigerator. Each photon which gets stopped in the HgTe absorber raises the temperature of the absorber by ~ 1 mK. The actual temperature rise depends on the photon energy. The XRS thermometry is accurate enough to measure the temperature to give us our very high X-ray photon energy resolution. For more details on the design and construction of XRS, see Kelley *et al*, 1999.[2] Given a suitable interpretation, the spectra will describe various interesting physical environments of astronomical sources. The spectra also carry signatures of the XRS instrument response. We must untangle the instrumental from the astronomical features of the spectrum.

Toward this end, we are engaged in a program to produce a photon response model which will predict a detection response for a given input photon spectrum. Key to this is a comprehensive calibration plan, both when XRS is on the ground and also when the instrument is in-flight. Here we will describe our ground calibration effort.

We have designed our calibration plan to address the most critical points of our detector model in a minimal amount of time. The ultimate scientific use of XRS defines these critical points. The strongest attribute of XRS to the scientific community is its very high energy resolution, particularly at high energies, where its throughput exceeds by an order of magnitude its nearest high energy resolution competitor, the AXAF high energy gratings. The gain function relating X-ray energy to pulse height directly affects the resolution. Other factors affecting the resolution are described in reference 3. Besides the core of the response, on the order of 1 percent of the detected flux is distributed broadly across the pulse height range due to electron and photon escape. The absolute quantum detection efficiency is also important, though the other instruments on ASTRO-E will probably do a better job at

Further author information: (Send correspondence to K.C.G.)
E-mail: kcg@milkyway.gsfc.nasa.gov

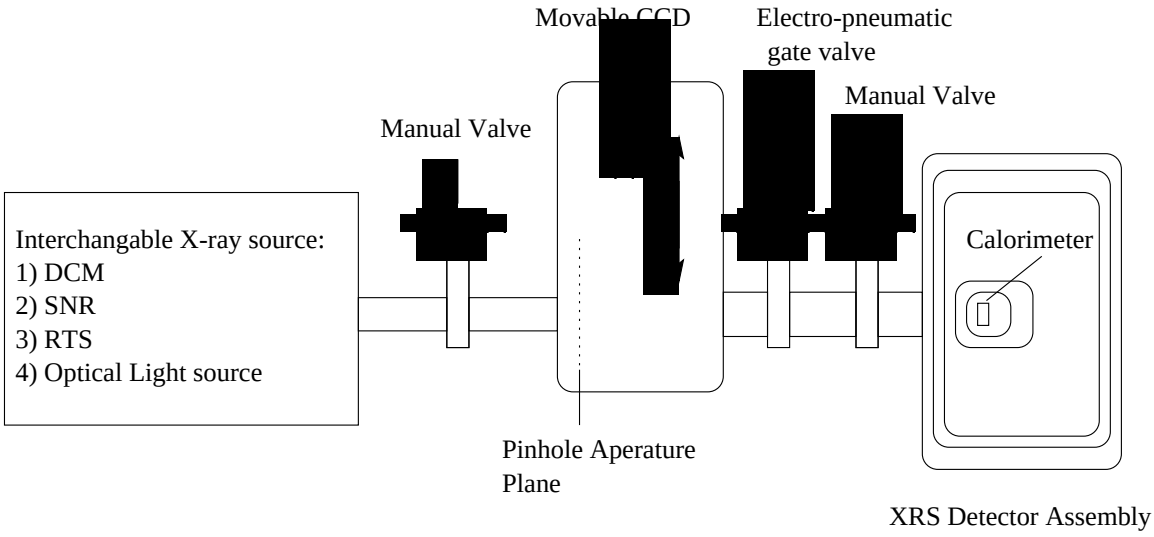

Figure 1. Basic schematic of the detector resolution and spectral redistribution

measuring flux, due to their larger field of view. The program of developing, building and debugging the flight instrument left us an extremely limited amount of time to perform a full calibration of the flight unit. Given this, we had to strictly limit the scope of our flight unit calibration to only the most essential measurements. Our ground calibration priorities are listed in table 1.

Table 1. XRS Ground Calibration Priorities

1) Energy Scale	knowledge to $\sim$ 1 eV
2) Resolution	knowledge to $\sim$ 1 eV
3) Coarse Spectral Redistribution	
4) Flux	strongly connected to XRT throughput

2. CALIBRATION HARDWARE

We have assembled a calibration facility to address the priorities listed in table 1. Our tools consist of various X-ray tubes, monochromators, spectrometers, radioactive sources, and reference detectors.

Our ground calibration activities are roughly divided between detector spectral calibration and optical blocking/thermal filter transmission calibration. We are calibrating gain, resolution, coarse and fine spectral redistribution issues, and flux in the detector calibration. While in the filter transmission work, we are basically calibrating a major component of the soft X-ray throughput.

The detector calibration is a major effort involving engineers, technicians, scientists and management. For XRS, calibration was worked into the critical path toward instrument delivery. As in most calibrations, we only had limited time to do our work within a few well defined windows. To optimize this part of the calibration, we built a setup which offered maximum flexibility with strong safeguards to protect the instrument from accidental damage.

2.1. The CCD Reference Chamber

We have constructed an X-ray CCD camera and chamber which we use for a number of purposes. It was designed to serve as a reference detector for the absolute flux calibration of XRS. Collimated X-rays from a monochromator or other type of source enter one end of the chamber. A movable X-ray CCD would either intercept and measure the beam or allow it to pass through and land on the XRS detector. Between the entrance of the chamber and the

CCD focal plane is an aperture plate containing various small (25 to 500 microns) pinholes. The plate is attached to a two-dimensional translation stage which allows motion orthogonal to the X-ray beam. With the plate, we can map a projected image of the XRS focal plane on the CCD. The map allows us to compare the flux measurements of the CCD with what XRS detects to back out the absolute flux calibration. The aperture plate also allows us to study some of the spatial dependence of the spectral redistribution of the XRS detectors.

The chamber has its own vacuum pumping system. The entrance port is gated with a manual gate valve. The exit port has an electro-pneumatic gate valve which is triggered to shut if the chamber pressure rises above an adjustable threshold or if the power goes out. The exit port serves as a safeguard for the flight detector system it would calibrate.

The CCD used is an *ASCA* engineering model X-ray CCD made by Lincoln Labs and MIT. It is a frame transfer device with 420×420 27 micron pixels in its imaging array. The electronics used to read it out are engineering *ASCA* instrumentation. More details can be found in Gendreau[4] and Burke *et al.*[5]

During the calibration of the flight unit, we did not, in fact, have time to do an absolute flux calibration. At this time, the CCD reference chamber was used to verify the functioning of the monochromators and to safeguard the vacuum integrity of the flight detector dewar system. This year we plan on doing a complete calibration of the flight spare system, using all the capacity of the reference chamber.

The CCD reference chamber is also used to image a reflection grating spectrometer's (described below) output during our filter calibration. Here, the energy resolution of the CCD is used to separate the various orders from the grating output.

2.2. The Double Crystal Monochrometer (DCM)

The National Institute of Standards (NIST) at Gaithersburg designed and made our Double Crystal Monochrometer (DCM). It consists of a multi-target, water-cooled electron impact x-ray tube (max power = 75 watts) that shines X-rays through a slat collimator (divergence ∼.3 mrad) toward a pair of Bragg crystals that select the X-ray energy to about 2 eV (depending on the crystal pair). The crystals are mounted on 2 rotating turrets. There are 5 crystal pairs to use: Si 400, Ge 111, KDP 011, RDP 001, and a ∼ 50 angstrom period multilayer. The multilayer had a very broad rocking curve and was not used. The remaining 4 crystals allow the DCM to cover from 1 to 15 keV.

Mechanical problems with the NIST design made the absolute energy scale difficult to predict. Also, the low throughput of the system and weak X-ray source forced us to do most work near characteristic lines. In practice, we used the DCM near characteristic lines after doing a local energy scan to determine the absolute output energy. The actual resolution of the DCM was verified in this way.

We used the DCM to constrain the resolution and coarse spectral redistribution parts of our detector model at high energies.

2.3. The Surface Normal Reflection Monochrometer (SNR)

Hettrick Scientific designed and made our Surface Normal Reflection Monochrometer (SNR). It consists of a "Manson type 2" electron impact source (power ∼ 5 watts) which shines X-rays through an adjustable entrance slit onto a collimating mirror which passes the collimated beam to a 7 inch diameter reflection grating which selects the X-ray energy and passes the photons through an adjustable exit slit. The SNR is a different type of reflection grating monochrometer in that the grating is rotated about the surface normal. This gives us a constant graze angle off the grating. More details can be found in Hettrick, 1992.[6] The SNR performs well from about 200 eV to about 2 keV with an energy resolution that varies from about 0.2 to 2 eV.

We used the SNR to constrain the resolution and coarse spectral redistribution parts of our detector model at low energies.

2.4. The Trufocus Continuum X-ray Source and the Rotating Target Source (RTS)

We used a air cooled electron impact x-ray source (power ∼ 2 watts) made by TruFocus (model TFS-5109) for a number of detector calibration tasks. The electron target in this source is Tungsten, which yields a strong continuum due to electron bremsstrahlung. Typically, we would operate this tube at 22 keV. We use this source in two different ways. Sometimes we shine the tube directly at our detector, so we get a continuum spectrum. The primary purpose for this mode of operation is to model the detector's high energy efficiency by measuring the strengths of the mercury

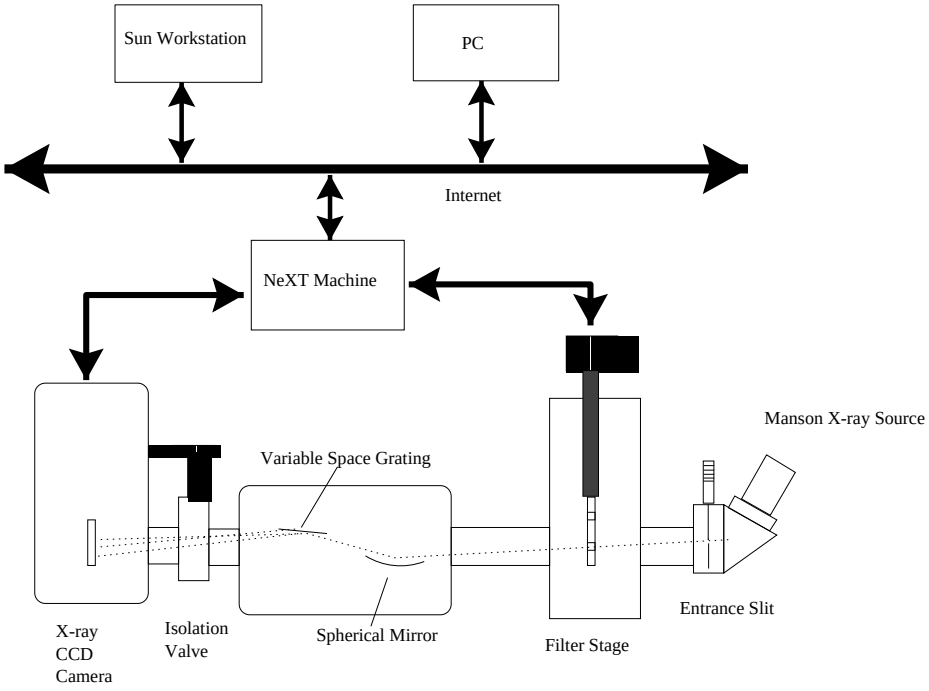

Figure 2. Schematic of the edge spectrometer filter transmission measuring system. A Manson X-ray source shines through a 20 micron wide slit. The x-rays then pass through a point where a filter can be inserted or removed. The x-rays then bounce off a spherical mirror and the grating to be intercepted by the CCD.

L edges (at $\sim$ 12-15 keV) of the HgTe X-ray absorbers of the XRS detector. We also use this source in an indirect way by shining the continuum X-ray output onto various targets to generate fluorescent characteristic X-ray emission lines. We have a target wheel containing 8 samples (Mo, Nb, Y, Zn, Cu, Cr, V, and Ti). As the wheel rotates (1 rotation in about 15 seconds), we get a time series of X-ray lines from 4.5 to 20 keV. This proves to be very useful to study the nonlinear gain of our system. When we use this source, we place a 0.005 inch thick Be window across the flange of the reference chamber where we would normally connect a monochromator.

2.5. The Edge Spectrometer (ES)

Hettrick Scientific designed and built our edge spectrometer (ES). The ES is a variable line-spaced grating spectrometer similar in design to the spectrometer on board EUVE.[7] In the ES, a Manson electron impact X-ray source illuminates an adjustable slit (width = 20 microns). X-rays pass through the slit onto a spherical mirror and then off a variable line space grating. The line spacing on the grating is designed to give a flat plane where the grating equation is satisfied. This is unlike the usual "Rowland circle" in a conventional grating. The plane that the grating projects its X-ray spectrum on is read out by an X-ray CCD (the CCD reference chamber described above). The CCD has an energy resolution that is adequate to separate the various spectral orders from the grating. The CCD's position resolution enables the high spectral resolution of the grating. In first order, we are achieving better than 0.5 eV FWHM energy resolution with this system. Our system is optimized to cover the oxygen K-edge in first order and the aluminum K-edge in third order. More details on the variable line-space grating spectrometer can be found in reference 8.

We use the ES along with a computer controlled filter translation stage to measure the transmission of our thermal/optical filters. See figure2 and 9 for more details. Once a filter is installed, the system runs automatically for about 1 week to obtain our high energy resolution transmission results.

3. THE GROUND CALIBRATION

On the ground, there have been several periods where we performed calibration activities. We outline these below and show some of the results.

3.1. GSFC, Winter 1997-1998

During the winter of 1997 to 1998, we had a 19 day period to calibrate the response of what was then the flight detector. This detector ended up not being the flight detector, due to engineering difficulties. In any case, this experience proved very useful as a shakedown test for all our calibration equipment.

3.2. GSFC, Winter 1998-1999

During the period from mid December to mid January, we had an opportunity to calibrate the spectral response of the flight detectors. Using the setup shown in figure 1, we did the following:

- Performed a general checkout of the instrument, once the detector cryogenic system was fully operating. This involved using an ^{55}Fe source in front of a beryllium window mounted to the entrance flange of the CCD reference chamber to determine the optimal bias level for the detectors. Here we maximized the resolution as a function of the bias level. We also measured current-voltage curves and system noise, both of which are important factors in our resolution model. More details can be found in reference 3.
- Derived the gains and optimized the thresholds and acceptance windows of the anti-coincidence detector behind the calorimeter detectors with an 241Am source.
- Checked the ability of the thermal/optical blocking filters to stop optical light by mounting an optical viewport to the entrance of the CCD reference chamber and flooding the system with strong optical light.
- Attached the DCM to the entrance flange of the CCD reference chamber to perform resolution and other spectral redistribution measurements of the calorimeter at the following energies (in keV): 6.4, 9.88, 8.045, 4.5, 5.4, and 8.635. During this time, we were also debugging the noise, changing instrument software, adjusting X-ray intensities, changing pulse templates (and thus the gain), experimenting with partially illuminating pixels, and slightly modifying cryogenic conditions for parts of the experiment. This made it difficult to compare results, but did bring out some unexpected effects which will improve our detector model.
- Exchanged the DCM with the SNR to make measurements at 0.525 and 1.488 keV Again, we varied several parameters during these measurements.
- Exchanged the SNR with the RTS/Continuum source to measure gain at several detector temperatures and the magnitude of the mercury L edges (at 12.28, 14.2 and 14.8 keV). In figure 3, you will see an example of the type of gain information we can get with the RTS. In figure 4, you will see the spectrum we obtain with the RTS rotated into "continuum" mode, where we derive the detector's contribution to the high energy flux calibration.

With this calibration, we achieved several of our goals. For example in figure 5, we have histograms of our measured resolutions at a few energies. Figure 6 shows a comparison of one of our spectral redistribution models compared to actual data. The model includes both photon escape and electron (photoelectron and Auger electron) escape.

We also encountered several unexpected gain and spectral redistribution effects in our calibration. We have working models and understand some of these effects. We also understand that our ground calibration of the flight sensors does not completely characterize the phenomena we see.

One of the gain effects we noticed were infrequent "glitches" in the gain. Figure 7 shows a typical glitch event as a sudden loss of gain in a pulse height versus time plot. In a glitch, all the pixels suffer the sudden loss in gain. It is as if the whole detector got slightly warmer. The gain loss slowly goes away on the time scale of several minutes. They occur approximately once every 2-4 hours. Our working model for this phenomenon is that high energy particles or photons are interacting with our detector board and heating the board a few millikelvin. The heat goes away slowly into our heat sink. We are expecting this to be a small effect in orbit, as our measured rate on the ground is so

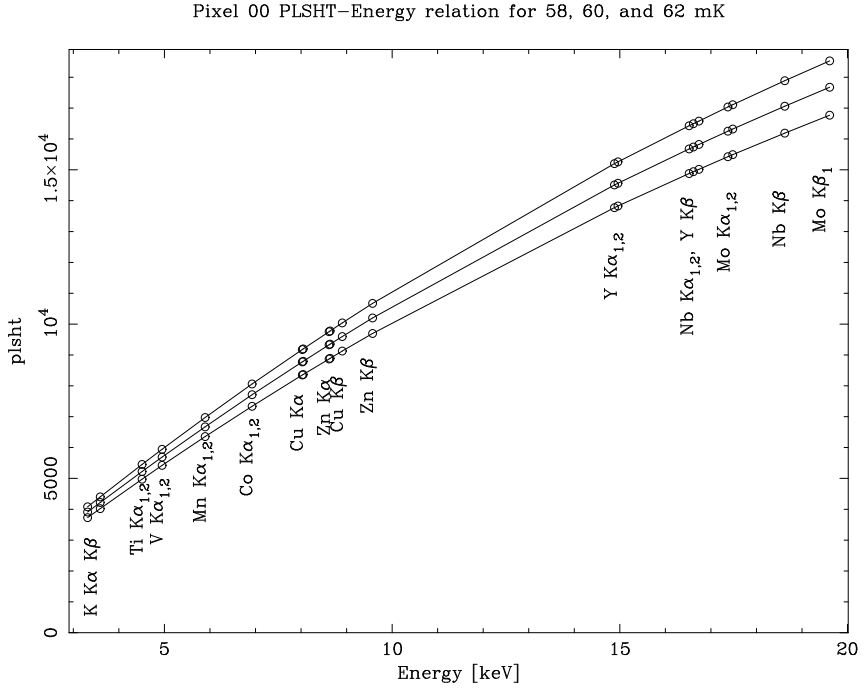

Figure 3. Pulse height vs energy for pixel 0 at three different temperatures from data taken with the RTS. The RTS provides gain information from 4.5 to 20 keV.

small compared to the expected fluence of minimum ionizing muons at sea level. However, we are still working on the data.

We also found slight rate dependences in the gain. As the counting rate varies from about 1 to 3 counts/sec/pixel the gain at about 8 keV would drop by about 0.03 % (or about 2 eV at 8 keV). We have done more analysis of this data and now believe that this is due to a "hot" pixel effect. As the rate increases, it becomes more likely that an event will occur while a pixel is still warm from a previous event. This results in a slight decrease in the gain due to the temperature dependence of the detector response. Since all our events are time tagged to ~10 microseconds, we can correct for this.

The spectra resulting from monochromatic X-rays striking pixels include a narrow gaussian feature with most of the counts. Our resolution numbers are the quoted FWHMs of this primary spectral redistribution filter. Some fraction $\sim < 1$ % of the counts make up a low energy tail due to electron and photon escape, as expected. However more than half of the pixels exhibit an unexpected spectral redistribution feature which we call the "hard tail". The hard tail is a strong (up to 25%) enhancement just to the high energy side of the primary sharp gaussian peak in our response- see figure 8. On the pixels which show this, the feature scales with energy and appears to be dependent on what part of the pixel is illuminated with X-rays. It is as if some part of some pixels have different photon thermalization properties. For our flight unit, we could only make a rough assessment of the position dependence by driving the sharp image of the DCM across some pixels to make a "knife edge" like measurement. We do not have a complete understanding of what is causing this. We expect that our flight spare calibration will be useful to sort this out.

3.3. Filter Calibration

During the times we are not calibrating our calorimeter detectors, we use the ES and the CCD reference chamber to measure the soft x-ray transmission of the optical blocking filters. See figure 9 for an example of the quality of these measurements. In this calibration we found discrepancies between the filter manufacturer's mesh specifications and our actual mesh transmission. We also calibrated the buildup of aluminum oxide on the filters. See ref 9 for more details.

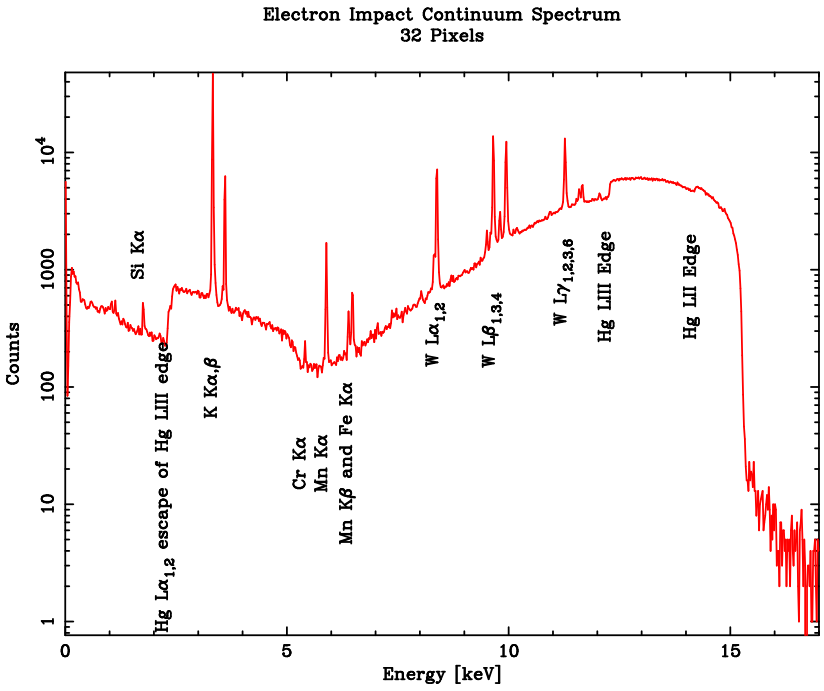

Figure 4. The XRS spectrum of the continuum source clearly shows the mercury L edges, which predict the detector component to the high energy efficiency of XRS. Also visible are lines from the onboard ^{55}Fe and ^{41}Ca calibration sources and W and Cu lines from the source itself. The spectrum is absorbed at low energies from traveling through about 1 meter of air, a stack of aluminum foils, and a beryllium window.

3.4. Flight Spare Calibration

During the summer and fall of 1999, we are planning on doing a more complete calibration of our flight spare system for XRS. In this calibration, we will more closely examine the spatial dependencies we found in the flight unit using the aperture plate in the reference chamber. The goal will be to understand the underlying physical mechanism of the hard tail so that we can make reasonable assumptions about the flight unit for which we did not have the time to do such a full calibration.

3.5. Japan, Summer 1999

During the 1999 summer, we expect to have approximately 2 weeks to perform a number of performance verification and calibration experiments in Japan with the XRS instrument more fully integrated. The purpose of these experiments will be to better understand the gain of our detectors. In these experiments, we will use both the onboard radioactive calibration sources and also the RTS. We expect the gain to change as we make optimal pulse templates for the flight detectors appropriate for the noise environment of the satellite. Measurements made at GSFC are somewhat clouded by the fact that our ground support equipment puts out a particular noise signature which will be different from that on the satellite.[3] It is very possible that this additional calibration of the exact gain function will still be insufficient for the actual in orbit performance.

4. EXPECTED IN-FLIGHT CALIBRATION PROGRAM

The Astro-E launch is set for January of 2000. Once in orbit, the satellite undergoes a checkout for about 2-3 weeks. Once this is done, we will open the XRS gate valve. We will give XRS a brief checkout, then it will proceed onto the rest of its scientific program.

For this door opening, XRS will be pointed at a supernova remnant called E0102 in the Small Magellanic Cloud. E0102 is a stable, time constant source with a number of low energy emission lines which makes it ideal as a monitor

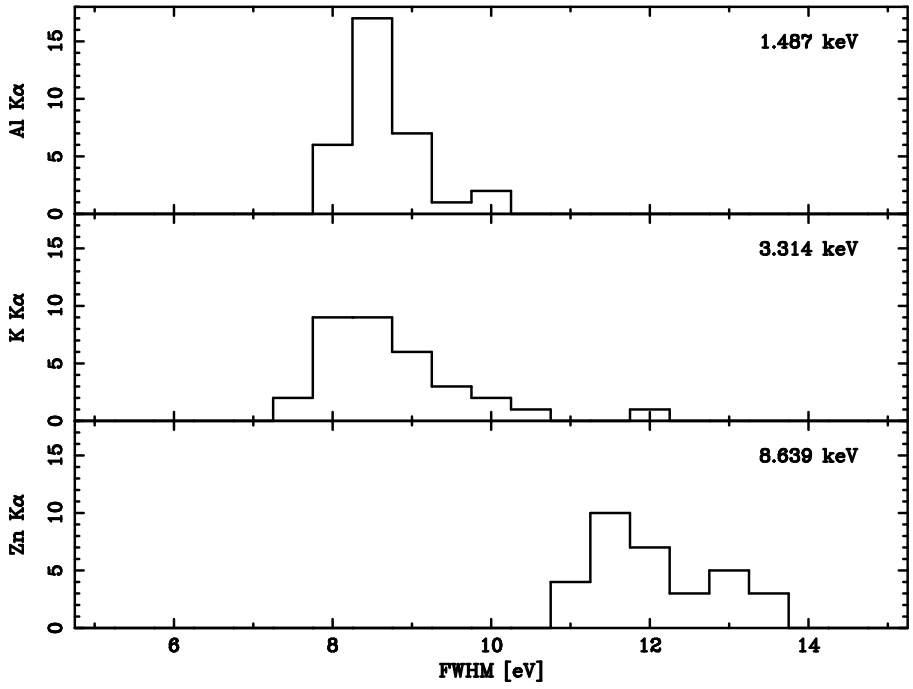

Figure 5. Histograms of measured resolutions at three different energies.

for ice buildup or evaporation from the cold optical blocking filters that stand in the optical path of the instrument. See figure 10 for a simulated XRS observation of E0102. XRS will revisit E0102 about 1-2 months later to look for any difference in the intensities of the low energy lines.

Next, Astro-E will look at the Perseus cluster of galaxies, where we will use the high energy iron K lines of Perseus to cross calibrate the highly nonlinear gain of XRS with the much simpler gain of the 4 X-ray CCD detectors (the XIS instrument) also flying on ASTRO-E. Since gain is so important, we will use other means to calibrate it, including observations of other objects and detection of the nickel K absorption edge in the XRS filters.

We will verify the ground resolution calibration by fitting the (relatively) simple line profiles for the on board radioactive calibration sources (^{55}Fe and ^{41}Ca). We may also make use of any other instrument background lines that we may encounter in orbit.

The absolute flux calibration will be more difficult, since it will involve understanding the X-ray telescope focusing the X-rays onto XRS. The point spread function is somewhat large compared to the size of the XRS array. This forces the flux calibration to require a very good knowledge of the energy dependent shape of the PSF. Clearly, the validity of the entire telescope model (geometric arrangement, surface roughness, optical constants, thermal shield parameters, ...) is essential to an accurate absolute flux calibration. In orbit, apart from icing measurements using E0102, the bulk of the in-flight flux calibration program will be driven by XRT issues. Relative calibration of the XRS-XRT system to the CCD-XRT systems (the XIS instruments also on board Astro-E) will be very important. The XIS instruments have a field of view much bigger than the PSF- so at least PSF issues will be minimal for the XIS compared to the XRS. It is not completely clear exactly how the PSF of the XRS telescope will be measured.

It is important to remember that XRS is a new type of instrument, and that, like in other experiments, the calibration is a difficult but necessary part of understanding the data. We have made the best effort we could on the ground to calibrate the instrument given the time available, but there is no doubt that there will be unexpected effects seen during its in-orbit use. We will continue to try to understand the instrument in-flight and the spare on the ground.

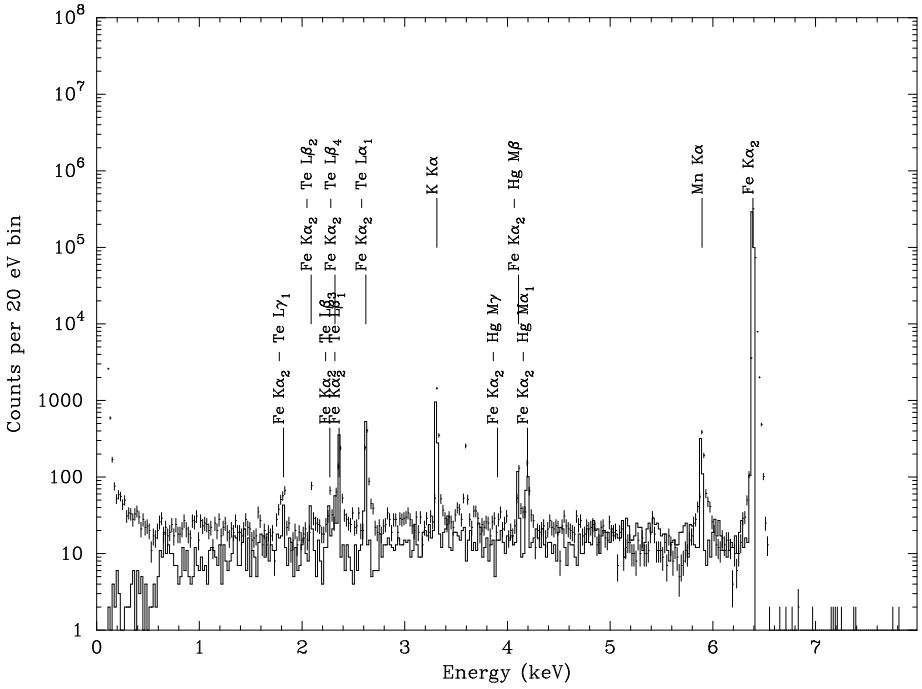

Figure 6. A comparison of data taken at 6.39 keV and a model for the coarse spectral redistribution- including electron and photon escape.

ACKNOWLEDGMENTS

We would like to thank Dave Bloom and the GSFC I&T staff, Susan Breon and the GSFC Code 713 Cryo branch, John Gygax, Regis Brekoski, Scott Murphy, Fred Finkbeiner, and everyone else who helped make this research possible.

REFERENCES

1. Y. Ogawara, "The Astro-E mission," in *Proc. of IAU Symposium no 188, Kyoto*, 1998.
2. R. L. Kelley *et al.*, "The Astro-E high resolution x-ray spectrometer," in *these proceedings*, *Proc. SPIE* **1999**, 1999.
3. C. K. Stahle *et al.*, "The design and performance of the Astro-E/XRS microcalorimeter array and anti-coincidence detector," in *these proceedings*, *Proc. SPIE* **1999**, 1999.
4. K. C. Gendreau, *X-ray CCDs for Space Applications: Calibration, Radiation Hardness, and Use for Measuring the Spectrum of the Cosmic X-ray Background*, MIT PhD. Thesis, Cambridge, 1995.
5. B. Burke, R. Mountain, D. Harrison, M. Bautz, J. Doty, G. Ricker, and P. Daniels *IEEE Trans. on Electon Devices* **38, no. 5**, p. 1069, 1991.
6. M. C. Hettrick, "Surface normal rotation: a new technique for grazing incidence monochrometers," *Appl. Opt.* **31**, p. 7174, 1992.
7. M. C. Hettrick, S. Bowyer, R. F. Malina, C. Martin, and S. Mrowka, "Extreme ultraviolet explorer spectrometer," *J. Opt. Soc. Am.* **68**, p. 1106, 1978.
8. M. C. Hettrick and S. Bowyer, "Variable line-space gratings: new designs for use in grazing incidence spectrometers," *Appl. Opt.* **22**, p. 3221, 1983.
9. M. D. Audley, K. C. Gendreau, C. Fleetwood, R. Keski-Kuha, J. Tveekrem, K.A.Arnaud, K. Boyce, R. Fujimoto, Y. Ishisaki, R. Kelley, T. Mihara, K. Mitsuda, F. Porter, C. Stahle, and A. Szymkowiak, "The Astro-E/XRS blocking filter calibration," in *these proceedings*, *Proc. SPIE* **1999**, 1999.

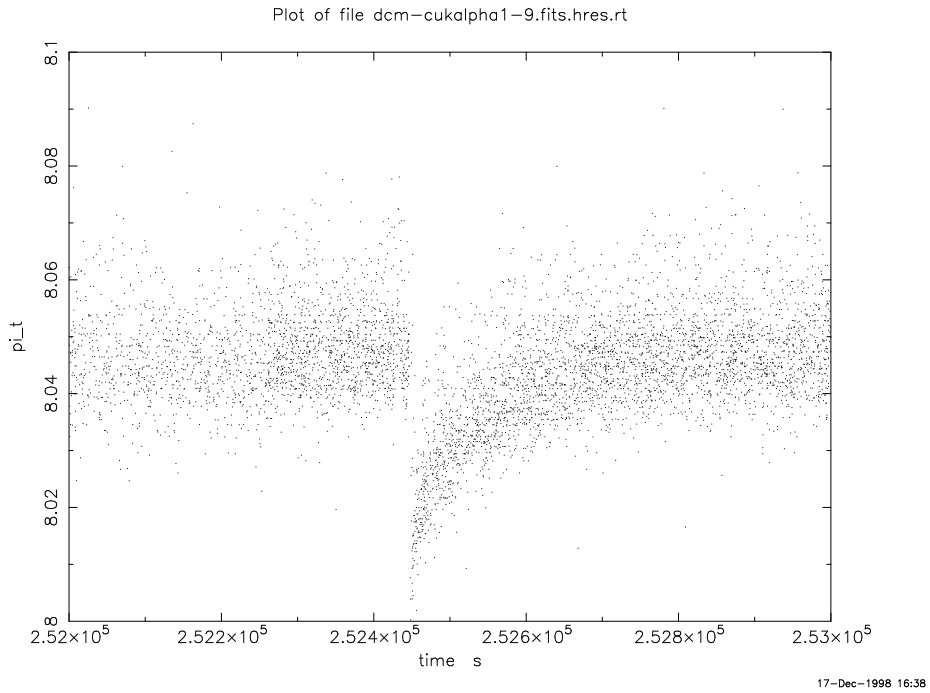

Figure 7. A "glitch" in a pulse height vs time plot.

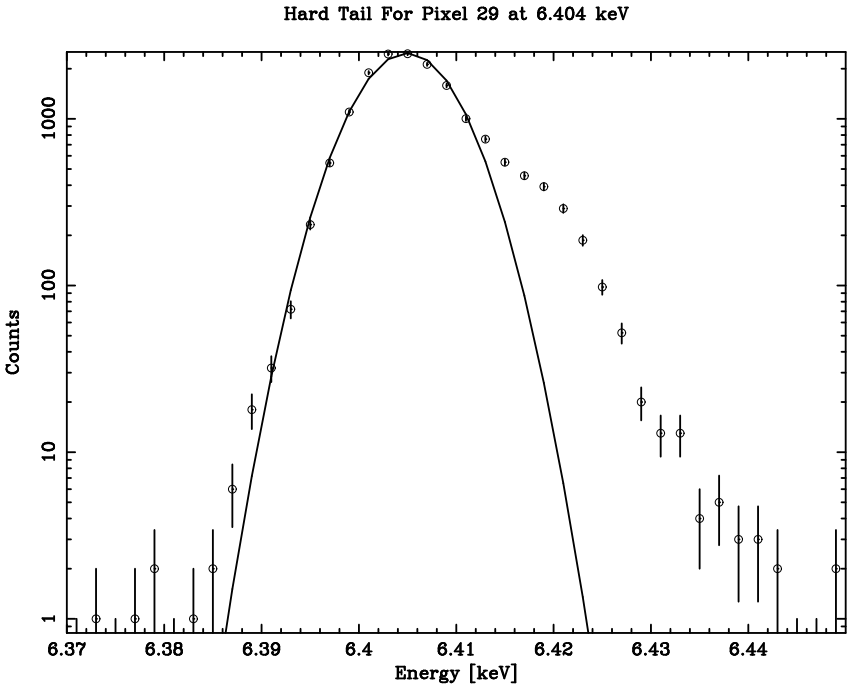

Figure 8. A typical Hardtail.

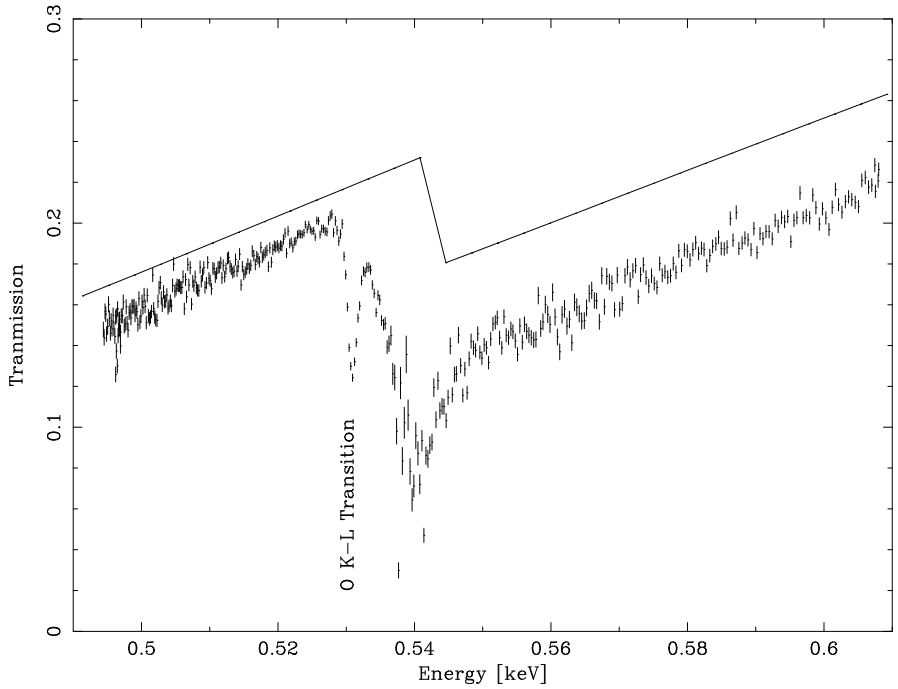

Figure 9. The oxygen edge region of a stack of calibration filters calibrated in the ES system. Note the sharp oxygen K-L absorption feature. Similar data was taken, in parallel to this, from ∼1 keV to ∼1.2 keV and across the aluminum K absorption edge. The solid line is a simple model based on the Henke data base.

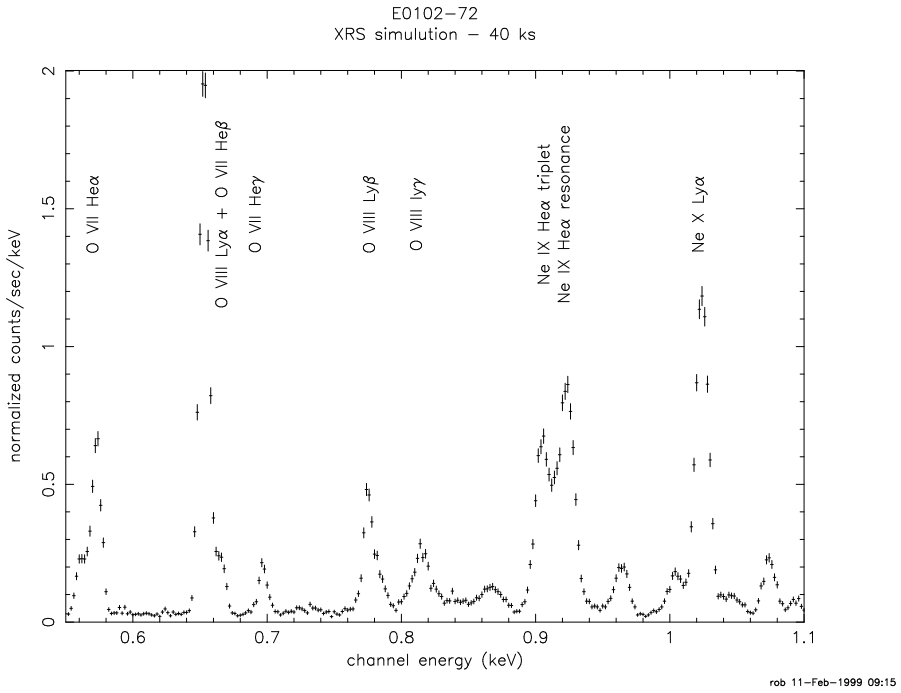

Figure 10. A simulated ASTRO-E/XRS spectrum from a 40 ksec observation of the supernova remnant E0102. Since E0102 is expected to be stable over the XRS mission life, any changes in the low energy line intensities over time will indicate a change in XRS low energy quantum efficiency- probably due to ice buildup or evaporation.